Dynamics of the Soft Wall Bunimovich Stadium

Sune Hørlück

Exam Report for

Classical and Quantum Chaos

by Predrag Cvitanovic.

spring 1995

September 9, 1995

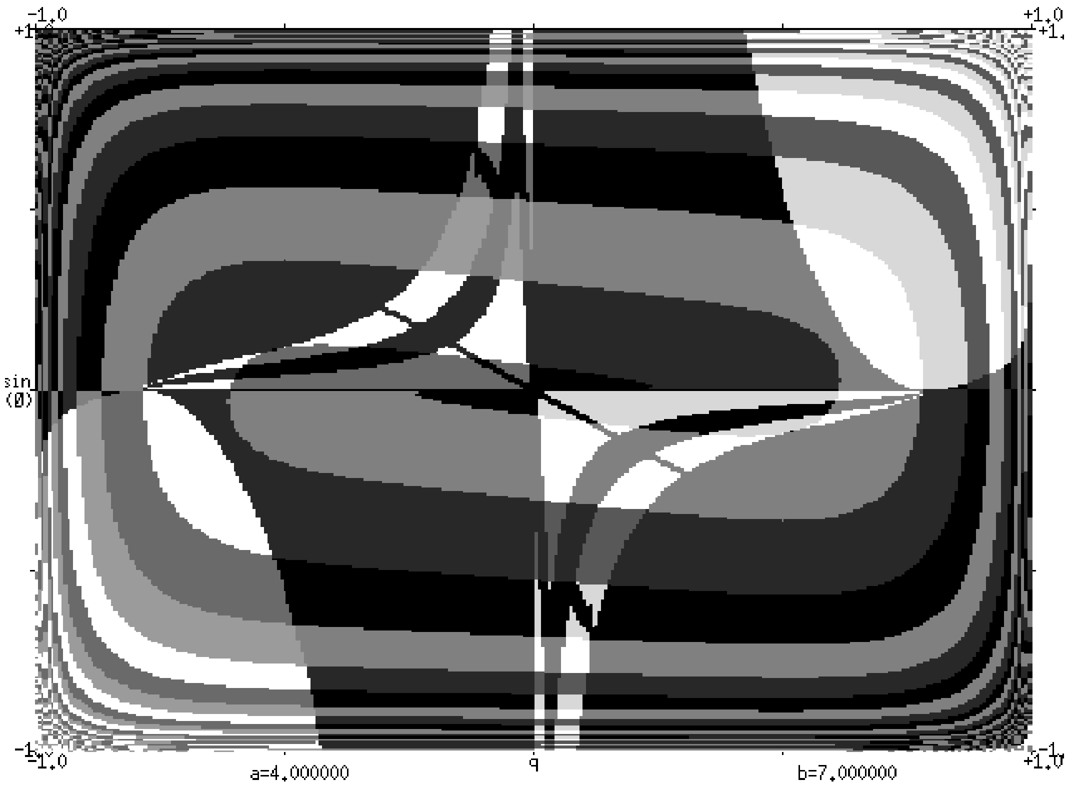

Contents

1 Introduction

The subject of the present examination is the Soft Wall Bunimovich stadium; a Hamiltonian system which should be seen as a generalisation of the hard wall stadium much studied in the literature, and the subject of a project parallel to this one by Jonas Lundbæk Hansen.

The hard wall Bunimovich stadium(1) has established it self as the standard example of a non escaping 2D billiards with convex bouncing surfaces (from the point of view of the ball). This together with a set of C^2 discontinuities in the 'corners' causes the system to have rather complicated symbol dynamics and dynamical pruning rules. The soft wall stadium with sides rising as polynomials r^b gives the gives the hard wall case in the limit $b \to \infty$ and thus examinations of systems with higher b's are in some sense Hamiltonian pre-states of the hard wall case.

The aim of this project of to establish working simulations of the particle motion in the soft wall, establish estimates of the lyapunov exponent and its dependence on system parameters based on the 'classical' methods, examine properties of the stable/unstable manifolds, examine the possibilities of defining a sensible type of symbol dynamics (based on the ones proposed by others for the hard wall stadium) , determine some ensemble of periodic orbits and finally attempt to apply the methods of periodic orbit theory to extract characteristic quantities of the system.

2 System Description

The hard wall Bunimovich stadium is the point of departure of this project a system description takes its logical point of departure in the hard wall case: two semicircles with radius 1 are connected by two straight walls of length $2a$ yielding a C_{2v} symmetry (symmetry under reflection in x-axis, y-axis and rotations of π. The dynamics of a particle bouncing within this closed, concave system is the subject of examination. Apart from linear divergence during free flight (due to different orientations of the momentum vector) all dynamics of this system takes place at the boundary. The boundaries has C^2 discontinuities in the points $(\pm a, \pm 1)$ which will later be shown to be of great significance to the dynamics. The Stadium can also be considered as the elementary cell in an unbounded version (a washboard system) consisting of two facing rows of semi circles. As can be seen from the system description below this kind of generalisation is irrelevant for the present system and will not be made object of examination.

The system presently under study replaces the flat bottom and the vertical reflecting walls with a potential rising from 0 at the line between $(-a, 0)$ to $(a, 0)$ to a value of 1 along the points corresponding to the hard wall stadium boundary confining the Hamiltonian particle to motion within the same area as in the hard wall case. This seems to suggest a potential depending on r being

$$r = y^2 + \left(\begin{array}{cc} (x+a)^2 & r \leq -a \\ 0 & r > -a \text{ and } r < a \\ (x-a)^2 & r \geq a \end{array} \right) \tag{1}$$

of cause it would be nice to get rid of the square roots, and this i achieved by using r^2 as our intermediate variable. this yields a potential $V(r^2)$, $r^2 = r(x,y)^2$ with gradient and Jacobian (the function $V(r^2)$ is of cause assumed to be 2 or more times differentiable)

The dynamics of the system is determined by the Hamiltonian equations of motion. (All simulated particles are assumed to have mass 1 and energy 1 corresponding to the potential at the boarder.) with $\vec{x} = (x, y, p_x, p_y)$ we thus have the

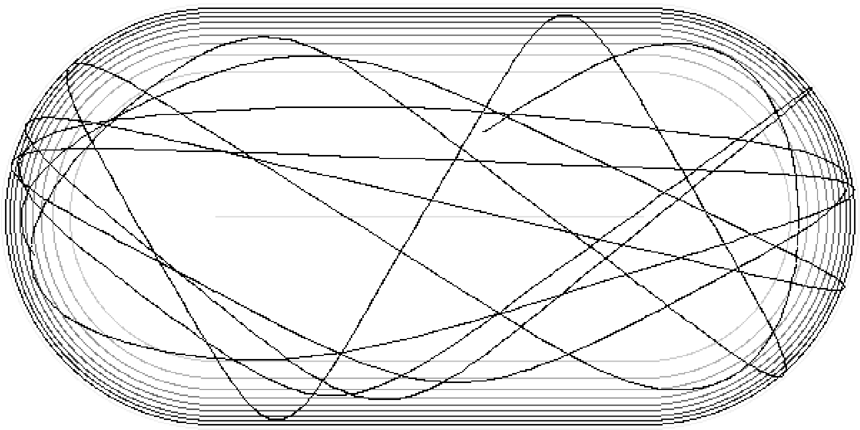

Figure 1: Trajectory for a=1, b=6 notice level curves for the potential at 10%,20%,...

equation of motion:

$$\frac{d}{dt}\vec{x} = F(\vec{x}) = \begin{pmatrix} p_x \\ p_y \\ -2V'(r^2)z \\ -2V'(r^2)y \end{pmatrix} \tag{2}$$

where z is given by

$$z = \begin{pmatrix} x+a & x \leq -a \\ 0 & r > -a \, and \, r < a \\ x-a & r \geq a \end{pmatrix} \tag{3}$$

Thus we get the Jacobian

$$J(\vec{x}) = \frac{\partial F(\vec{x})}{\partial \vec{x}} = \begin{pmatrix} 0 & 0 & 1 & 0 \\ 0 & 0 & 0 & 1 \\ -\rho 2V' - 4V''z^2 & -4V''zy & 0 & 0 \\ -4V''zy & -\rho 2V' - 4V''y^2 & 0 & 0 \end{pmatrix}, \text{ where } \rho = 1 - \delta_{z=0} \tag{4}$$

As is easily seen this model also has discontinuities of the second derivative in the points $(+a, +1)$ and along the vertical lines connecting them (provided of cause that the value $V'(r^2)$ differs from zero in these points. Furthermore it would be convenient to have a potential with low values of V, V' and V'' for low values of r and radially rising values near r=1. A obvious choice is of cause $(r^2)^{b/2} or r^b$ for reasonably high values of b. This is indeed the only form of V implemented in this project (the existence of two parameters ensures more than enough work for a project of this size). For values of $b = 4, 6, 8, 10 \ldots$, only multiplication and addition is required in simulation which of cause makes these cases especially attractive. For values $b < 4$ the dynamics have too many pockets of quaziperiodicity etc. to resemble those of the hard wall stadium (especially for low values of a). For high values of $b \geq 10$ the implemented methods of simulation breaks down far too often. When the orbit crosses the mid line (either way) or the line where the semi circle starts, the values of y and $\sin(\phi)$ (where ϕ is the angle of the velocity vector) are determined through linear interpolation. The result is points in the three poincar/'e cuts:

Type 1 Entering the semi circle

Type 2 Exiting the semi circle

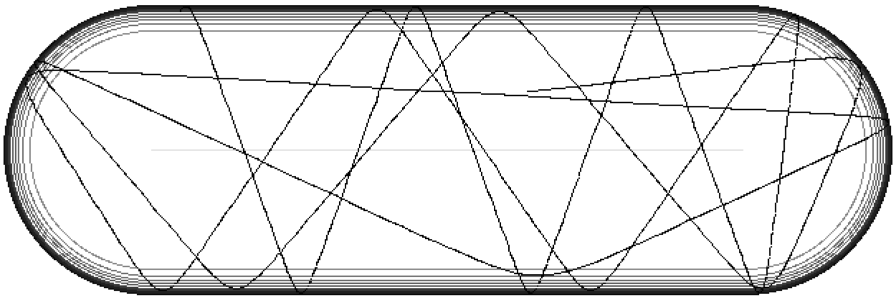

Figure 2: Trajectory for $a = 2.0, b = 12$.

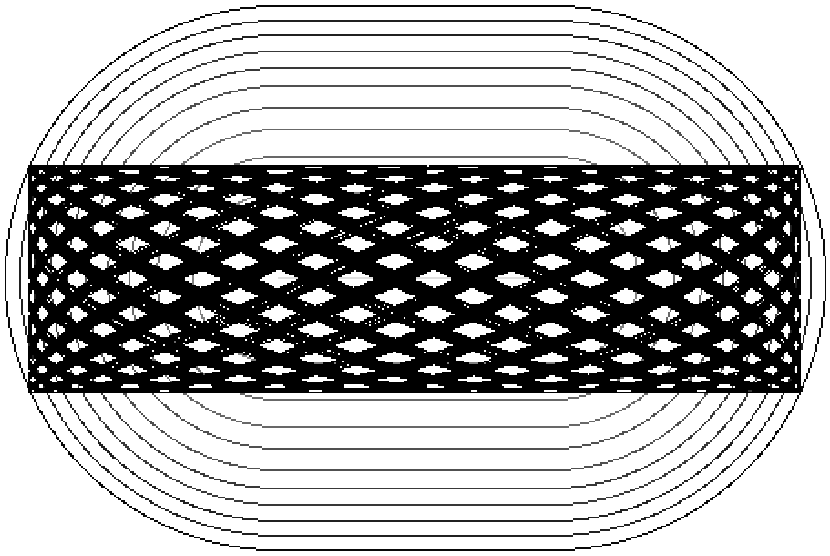

Figure 3: Trajectory for a=0.5 , b=2 . Notice quaziperiodicity .

Type 3 Crossing the y-axis

types 1 and 2 will prove to be important in the matters of symbol dynamics. They time reflect into one another. type 3 will prove to be important when it comes to search for periodic orbits with good symmetry properties.

During the early phases of the project different methods of simulation were tested; mainly based on the Numerical Recipes implementations of Bulirsch Stoer method of integration and the fourth order Runge Kutta method with a variable step size. The BS method had a high frequency of simulation breakdown apparently caused by the C^2 discontinuities at $x = \pm a$ (step size drastically decreased in this region. The RK4 method proved to be more stable, but even this method is somewhat unstable for values of b above 9. The use of 10 bytes floating point precision instead of 8 bytes ditto was tested, but the cost in simulation speed and software portability problems was so significant that this line of experimentation was aborted (for further details see Appendix A).

3 Instability / Lyapunov Exponents

The main emphasis of most examinations of chaotic systems is the determination of rate of divergence of nearby initial conditions. Exponential divergence is needed to have chaos (as a matter of definition), and the exponent in question is called the lyapunov exponent. This kind of divergence can not normally continue further than up to the characteristic size of the system: Either the dynamics are limited and the divergence will stop all together or the system allows escaping trajectories – in which case the divergence typically will enter a regime of linear divergence in which at least one of the particles are excaping. The lyapunov exponent λ could be defined:

$$|\delta\mathbf{x}(t)| = e^{\lambda t} \cdot |\delta\mathbf{x}(0)| \tag{5}$$

As described in the original (overhead photocopy) version of chapter 3 of the lecture notes on flows a system of Ordinary Differentiable Equations (Ode's) of the form $d\vec{x}/dt = F(\vec{x})$ can be Taylor expanded in small differences in initial conditions :

$$\frac{d}{dt}(\vec{x} + \delta\vec{x}) = F(\vec{x}) + \frac{\partial F(\vec{x})}{\partial \vec{x}}\delta\vec{x} + \dots \tag{6}$$

Ignoring the influence of the higher order terms (who ultimately kills any divergence at the length scale of the system) the actual starting size of $\delta\vec{x}$ is irrelevant: Only its relative growth rate is significant. The same can not be said of its orientation in phase space: Even though any initial orientation with components along directions[1] of consistent growth will eventually orient itself in these directions. The unknown influence of the transient period compromises the use of this method for determining the lyapunov exponent.

If on the other hand the integration above takes place for any orthogonal system of differences in initial conditions the numerically largest eigenvalue of the integrated $M(t)$ satisfies our requirements for a unique instability number of the trajectory $vecx(t), t \in [0, T]$. The differentiable equation takes the form

$$d/dtM(t) = L(x(t), y(t))M(t) \quad M(0) = I \quad (I_{ij} = \delta_{ij}) \tag{7}$$

With this method integration of motion involves the four variables of motion PLUS 16 elements of the M(t) matrix. But for a time independent flow with conserved energy we know, that at least two of the eigenvalues will have the value 1: a shift in initial conditions along the trajectory corresponds to a time shift which is not subject to divergence. Two close-by orbits with difference in energy will keep their energy difference and in the linear regime this too will correspond to a eigenvalue 1 footnote : time shifts along trajectories and energy shifts are obviously non parallel in timeindep. systems. The conservation of flow volume in Hamiltonian systems furthermore ensures $\det(M(t)\ ) = 1$, which causes the two remaining eigenvalues to take the form $\lambda, 1/\lambda$. Based on this knowledge a transformation of the above equation system can be performed leaving only a 2*2 matrix to be integrated $\tilde{m}. = \tilde{l} * \tilde{m}$ [Tan92]. $\tilde{l}$ here takes the form :

$$\tilde{l} = \begin{pmatrix} -(q^{-1})(h_x h_u + h_y h_v)(h_{xx} + h_{yy} - h_{uu} - h_{vv}) & q^{-2}[(h_x{}^2 + h_v{}^2)(h_{yy} + h_{uu}) + (h_y{}^2 + h_u{}^2)(h_{xx} + h_{vv})] \\ -((h_x{}^2 + h_y{}^2)(h_{uu} + h_{vv}) - (h_u{}^2 + h_v{}^2)(h_{xx} + h_{yy})) & (q^{-1})(h_x h_u + h_y h_v)(h_{xx} + h_{yy} - h_{uu} - h_{vv}) \end{pmatrix}$$

where h_i , h_{ij} are derivatives of the Hamiltonian H (u, v) are the momentum components and $q = |dH|^2$. (In general the expression is more involved)

This method only demands the integration of 8 equations, and after ended integration the eigenvalues of the 2*2 matrix $\tilde{m}(t)$ should be straight forward giving Λ and therethrough the lyapunov exponent $\lambda = ln(\Lambda)/T)$.

Estimates of the lyapunov exponent for the overall system at different values of a and b, can now be obtained using any of the above methods based on some randomly chosen set of initial conditions (Brute method) or by means of Periodic Orbit Theory (Elegant but troublesome to be discussed in following sections).

[1] The set of directions without such components have zero measure, and the growth direction eigenvectors are assumed to twist sufficiently slow for nice systems

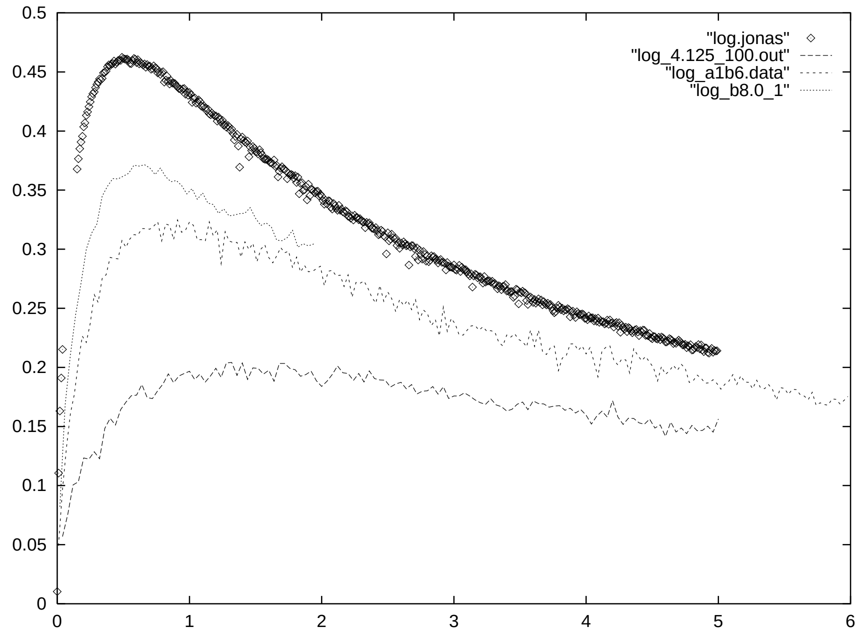

Figure 4: Diverging orbit lyapynov exponents as functions of a for b=4,6,8. Upper curve is the hardwall curve for comparison

A method that looks straight forward in theory is not necessarily easy implementable in simulation: The methods sketched above have during the project been attempted implemented with differing success. The method of differing orbits is crude, but its solely based on the well tested elementary 4d ODE integration together with appropriate schemes for renormalization of the difference vector (the orbit distance should never exceed $1.0 * 10^{-3}$) and for time syncronizing the evolution of the two orbits. This method is despite its crudeness and sensitivity to nonlinear effects used as the reference throughout this project: Neither the 4 vector or the 4×4 matrix are very convenient or elegant, and during the early phases of the experiment they proved hard to stabilise. Thus they have been dropped altogether. The 2×2 matrix was attempted implemented in different versions before I settled with the Tanner-form. The method has nice properties of elegance and dimensional similarity with the method used in the Hard Wall Stadium. BUT it has caused no end of trouble: It has proven very hard to stabilise either because of the discontinuities or some interplay potential in the semi circles. Only 4 days before the final delivery date it reached a stability good enough to allow the application of the numerical output in further calculations. Its success has been monitored through comparison with the results of the *parallel orbits* method. In Appendix C the instability factors obtained through the two methods can be made subject of examination. Note that for orbits whose semi circle bounces follows a radius the correspondence is good, whereas in other cases rather bad correspondences are seen; this will be made subject of further discussion in Section 5.

4 Orbit Theory

The dynamics of the hard wall Stadium has been proved to be almost everywhere chaotic[2] .The almost comes from a set of measure 0 - including *the periodic orbits.*

[2]the infamous vertically bouncing orbits will be ignored in the following

To some extend this alse seems to be the case too for the Soft Wall Stadium if b is not too low ($b > 4$)

At first it might seem counter intuitive to use such a un-typical subset of the trajectories in the studies of the general dynamics. Therefore this section is dedicated to the motivation of periodic orbit theory. It includes parts of Chapters 4 and 5 in the course material [Cvi95] relevant to the treatment of flows.

4.1 Evolution Operators

The fraction of initial x whose trajectories start out within a phase space region V and recur within that region at the time t is given by

$$\Gamma_V(t) = \frac{\int_V dx dy\, \delta(y - f^t(x))}{\int_V dx}\,. \tag{8}$$

Here $\delta(\cdots)$ is the Dirac delta function: for a deterministic flow the initial point x maps into a unique point y at time t. If the dynamics is bounded, and V envelops the entire accessible phase space, $\Gamma_V(t) = 1$ for all t. However, if there exists a finite region V such that a trajectory that exits V never reenters, the recurrence fraction necessarily decreases with time. Ignoring possible minute pockets of stability[3] we have a ergodic chaotic system with no escaping trajectories wherefore such complications can be ignored.

The kernel of (**??**) propagates densities of trajectories and is a representation of the Frobenius-Perron operator (**??**):

$$\mathcal{L}^t(y,x) = \delta\big(y - f^t(x)\big)\ . \tag{9}$$

for a (d+1)-dimensional continuous flow, $f^t(x)$ is the trajectory of the initial point x. More generally, we shall consider *evolution operators* $\mathcal{L}$ given by

$$\mathcal{L}^t(y,x) = g(x)\,\delta\big(y - f^t(x)\big)\ . \tag{10}$$

Here $g(x)$ is any weight multiplicative along the trajectory. We shall motivate introduction of such weights in a later subsection; for now it suffices to take $g(x) = 1$. The evolution operator propagates a density of initial conditions $\phi(x)$ to $\phi^t(x)$, the density at time t:

$$\begin{aligned}
\left(\mathcal{L}^t \circ \phi\right)(x) &= \int dy\, \delta\big(x - f^t(y)\big)\, \phi(y) \\
&= \sum_{y=f^{-t}(x)} \frac{\phi(y)}{|f^t(y)'|} \qquad\qquad \text{1-dimensional} \\
&= \sum_{y=f^{-t}(x)} \frac{1}{\left|\det \frac{\partial f^t(y)}{\partial y}\right|}\, \phi(y) \qquad d\text{-dimensional}\,.
\end{aligned} \tag{11}$$

Schematically, a linear operator has a spectrum of eigenvalues s_α and eigenfunctions $\varphi_\alpha(x)$

$$\left(\mathcal{L}^t \circ \varphi_\alpha\right)(x) = e^{-s_\alpha t}\varphi_\alpha(x)\,, \qquad \alpha = 0, 1, 2, \ldots$$

ordered so that Re $s_\alpha \le s_{\alpha+1}$.

Our hope is that perhaps all global averages of physical interest such as energy eigenvalues, resonances, fractal dimensions, and Lyapunov exponents can be extracted from the eigenvalues of evolution operators.

[3]for $b \ge 5$ I've seen no sign of their existence in my many simulations.

From now on we shall strive to make sense of the evolution operator $\mathcal{L}$ as a matrix. There are several standard methods of approximating $\mathcal{L}$ by a finite matrix $\mathbf{L}$.

In the *bruto insensitivo* approach, one subdivides the d-dimensional phase space into hypercubes $V_1, V_2, \cdots, V_{N^d}$ of volume $\epsilon = V/N^d$ and approximates $\mathcal{L}$ by the overlap integral

$$\mathcal{L}^t \to \mathbf{L}^t_{ij} = \int_{V_j} dx \int_{V_i} dx\, \delta\big(y - f^t(x)\big)\, g^t(x) \approx \big(V_i \cap f^t(V_j)\big)\, g^t_j\,, \tag{12}$$

where $V_i \cap f^t(V_j)$ is the fraction of initial volume V_j that lands in the cell i at time t, and g^t_j is an estimate of the weight $g^t(x)$ averaged over the initial cell $x \in V_j$. One then crosses one's fingers and hopes that as $N \to \infty$, the interesting part of the spectrum of $\mathbf{L}$ converges to the eigenvalues of $\mathcal{L}$.

More sensitive approaches expand the initial and final distributions ϕ, ϕ^t in a basis $\varphi_0, \varphi_1, \varphi_2, \cdots$ (orthogonal polynomials, let us say) and replace $\mathcal{L}^t(y,x)$ by its φ_α basis representation $\mathcal{L}^t_{\alpha\beta} =< \varphi_\alpha|\mathcal{L}^t|\varphi_\beta >$. The difficult art then consists in finding a 'good" basis for which finite truncations of $\mathcal{L}^t_{\alpha\beta}$ give accurate estimates of the eigenvalues of $\mathcal{L}^t$.

The problem with the bruto insensitivo attack on the problem is that it is blind; the grid knows not what parts of the phase space are more or less important, and not only that - at times the approach is plain wrong, yielding spurious eigenvalues. We shall do much better than that; we shall use the internal topology of the flow to give us both an invariant partition of the phase space and invariant measure of the partition volumes. We shall lean on the φ_α basis approach only insofar it helps us establish that the spectrum that we compute is indeed the correct one, and that finite periodic orbit truncations do converge.

4.2 Trace formulas

Our extraction of the spectrum of $\mathcal{L}$ commences with the evaluation of the trace

$$\mathrm{tr}\,\mathcal{L}^t \;=\; \int dx\, \mathcal{L}^t(x,x) \;=\; \int dx\, \delta\big(x - f^t(x)\big)\; \mathrm{tr}\, g^t(x)\,.$$

By the definition of the trace

$$\mathrm{tr}\,\mathcal{L}^t = \sum_{\alpha=0}^{\infty} e^{-s_\alpha t}$$

(we ignore for the time being the question of convergence of this sum), so if we can evaluate the above delta-function integral, we have a formula for eigenvalue sums. The $\delta(x - f^t(x))$ factor in the integral can only differ from 0 (given $t > 0$) on periodic orbits, giving the first indication of their central role.

As any point on a cycle returns to itself exactly at each cycle period, the eigenvalue corresponding to the eigenvector along the flow necessarily equals unity for all periodic orbits, and the trace integral $\mathrm{tr}\,\mathcal{L}^t$ requires a separate treatment for the longitudinal direction. To evaluate the contribution of a prime cycle p of period T_p, restrict the integration to an infinitesimally thin tube V_p enveloping the cycle, and choose a local coordinate system with a longitudinal coordinate $dx_\parallel$ along the direction of the flow, and d transverse coordinates $x_\perp$

$$\mathrm{tr}\,{}_p\mathcal{L}^t = \int_{V_p} dx_\perp dx_\parallel\, \delta\big(x_\perp - f^t_\perp(x)\big)\, \delta\Big(x_\parallel - f^t_\parallel(x)\Big)\;\;. \tag{13}$$

Let v the longitudinal variable to $dx_\parallel = v\, d\tau$. The integral along the trajectory yields a contribution whenever the time t is a multiple of the cycle period T_p

$$\begin{aligned}\int_{V_p} dx_\parallel\, \delta\Big(x_\parallel - f_\parallel^t(x)\Big) &= \sum_{r=1}^{\infty} \delta(t - rT_p) \int_p d\tau \\ &= T_p \sum_{r=1}^{\infty} \delta(t - rT_p) \ . \end{aligned} \tag{14}$$

Linearization of the periodic flow in a plane perpendicular to the orbit yields

$$\int_{V_p} dx_\perp \delta\Big(x_\perp - f_\perp^{rT_p}(x)\Big) = \frac{1}{|\det\left(\mathbf{1} - \mathbf{J}_p^r\right)|} \ , \tag{15}$$

where $\mathbf{J}_p$ is the p-cycle $[d \times d]$ *transverse* Jacobian matrix (this is why we chose to refer to the flow as $(d+1)$-dimensional), and we have assumed hyperbolicity, *ie.* that the magnitudes of all transverse eigenvalues are bounded away from unity. (keep in mind that even though our phase space flow formally 4-dimensional – the conservation of energy confines the flow to a 3-dimensional manifold whereby we get the $d = 2$)

Substituting (14)-(15) into (13), we obtain an expression for $\operatorname{tr} \mathcal{L}^t$ as a sum over all prime cycles p and their repetitions

$$\operatorname{tr} \mathcal{L}^t = \sum_p T_p \sum_{r=1}^{\infty} \delta(t - rT_p) \frac{\operatorname{tr} g_p^r}{|\det\left(\mathbf{1} - \mathbf{J}_p^r\right)|} \ . \tag{16}$$

A Laplace transform smoothes the above sum over Dirac delta functions and yields the *trace formula* for evolution operators:

$$\operatorname{tr} \mathcal{L}(s) := \int_{0_+}^{\infty} dt\, e^{st} \operatorname{tr} \mathcal{L}^t = \sum_p T_p \sum_r^{\infty} \frac{e^{sT_p r} \operatorname{tr} g_p^r}{|\det\left(\mathbf{1} - \mathbf{J}_p^r\right)|} \ . \tag{17}$$

4.3 Fredholm determinants

The problem with the trace formulas described so far is, that they diverge at the interesting values; divergence is a relatively problematic kind of characteristic behaviour compared with zeros etc. Furthermore the radius of convergence might hinder the determination of the eigenvalues beyond the first one. Inspired by the relationship $F(z) \to \infty \Leftrightarrow \exp(-F(z)) \to 0$ we turn our attention towards determinant formulas. For finite Matrices eigenvalues are normally determined af the zeros of

$$\det(1 - z\mathcal{L}) = \prod_\alpha (1 - z\lambda_\alpha) \ . \tag{18}$$

Given an infinite number of periodic orbits (as we are faced with – at least in theory) The Determinant is linked to the traces through

$$\log\det(1 - \mathcal{L}) = \operatorname{tr}\, \log(1 - \mathcal{L}) = \sum_{n=1} \frac{1}{n} \operatorname{tr} \mathcal{L}^n \ ,$$

For flows the Fredholm determinant takes the form

$$F(s) = \exp\left(-\sum_p \sum_{r=1}^{\infty} \frac{1}{r} \frac{e^{sT_p r} g_p^r}{|\det\left(\mathbf{1} - \mathbf{J}_p^r\right)|}\right) \ . \tag{19}$$

With z set to $z = e^s$, the Fredholm determinant (21) has the same form for both maps and flows. The trace formula (**??**) is the logarithmic derivative of the Fredholm determinant

$$\mathrm{tr}\,\mathcal{L}(s) = -\frac{d}{ds}\log F(s) \ . \tag{20}$$

Using the possibility to divide periodic orbits up in prime cycles and their repeats the following expression for the Fredholm determinant can be derived

$$F(s) = \exp\left(-\sum_p \sum_{r=1}^{\infty} \frac{1}{r} \frac{e^{sT_p r} g_p^r}{|\det\left(\mathbf{1} - \mathbf{J}_p^r\right)|}\right) \ . \tag{21}$$

Turning the definitions around the trace formula (**??**) can be viewed as the logarithmic derivative of the Fredholm determinant

$$\mathrm{tr}\,\mathcal{L}(s) = -\frac{d}{ds}\log F(s) \ . \tag{22}$$

Remembering that volume is conserved in a Hamiltonian flow such as ours (causing the determinant of the jacobiant to be 1) and using our earlier conclusion that only the two transverse eigenvalues can differ from 1, we conclude that we will have only one eigenvalue Λ with $|\Lambda| > 1$ which can be used to simplify the expression of $F(s)$ somewhat:

$$\frac{1}{|\det\left(\mathbf{1} - \mathbf{J}_p^r\right)|} = \frac{1}{|\Lambda|^r(1 - 1/\Lambda_p^r)^2} = \frac{1}{|\Lambda|^r}\sum_{k=0}^{\infty} \frac{(k+1)}{\Lambda_p^{kr}} \ . \tag{23}$$

Whereby

$$\sum_{r=1}^{\infty} \frac{1}{r} \frac{e^{sT_p r}}{|\det\left(\mathbf{1} - \mathbf{J}_p^r\right)|} = \sum_{k=0}^{\infty} (k+1)\log\left(1 - \frac{e^{sT_p}}{|\Lambda_p|\Lambda_p^k}\right) \ ,$$

and the Fredholm determinant rewritten as an infinite product over prime cycles

$$F(s) = \prod_p \prod_{k=0}^{\infty} \left(1 - t_p/\Lambda_p^k\right)^{k+1} \ , \qquad t_p = \frac{e^{sT_p} g_p}{|\Lambda_p|} z^{n_p} \ . \tag{24}$$

In such formulas, t_p is a weight associated with the p cycle (letter t refers to the 'local trace" evaluated along the p cycle trajectory), z is a formal parameter which keeps track of the topological cycle lengths, and the index p runs through all distinct prime cycles. We will use z to expand zeta functions and determinants, then set to $z = 1$ in calculations.

4.4 Dynamical zeta functions

As discussed above, one is interested only in the leading eigenvalue of $\mathcal{L}^t$, the size of the p cycle neighbourhood can be approximated by $1/|\Lambda_p|^r$, the dominant term in the $t \to \infty$ limit, where $\Lambda_p = \prod_e \Lambda_{p,e}$ is the product of the expanding eigenvalues of the Jacobian matrix $\mathbf{J}_p$. With ths replacement the Fredholm determinant (21) is thus approximated by the *dynamical zeta function*

$$1/\zeta = \exp\left(-\sum_p \sum_{r=1}^{\infty} \frac{1}{r} t_p^r\right) \ . \tag{25}$$

Resuming the logarithms as in (**??**) we obtain the *Euler product representation* of the dynamical zeta function:

$$1/\zeta(s) \ = \ \prod_p (1 - t_p) \ , \qquad t_p = \frac{1}{|\Lambda_p|} g_p \, e^{sT_p} \ . \tag{26}$$

The dynamical zeta function is useful because it also vanishes at e^s equal to e^{s_0}, the *leading* eigenvalue of $\mathcal{L}^t$, defined implicitly as the largest solution of either of the equations

$$F(s) = 0\,, \quad 1/\zeta(s) = 0\,. \tag{27}$$

4.5 Dynamical averaging

(very very shorthand - consult [Cvi95] chapter 5 for details.)

We now want to try and develope the orbit theory in a direction, where a suitable broad set of characteristic quantities of the system can be extracted. For the oprators coresponding to these quantities Φ, that must be along a trajectory it can be argued, that it is convenient to define a fredhold determinant of that observable

$$F(\beta, s) \;=\; \prod_p \exp\left(-\sum_{r=1}^{\infty} \frac{1}{r} \frac{e^{(\beta\cdot\Phi_p - sT_p)r}}{|\det\left(\mathbf{1} - \mathbf{J}_p^r\right)|}\right)\,. \tag{28}$$

In bouded systems we can now obtain the system averaged quantities – and their spread – of these operators through:

$$\left.\frac{\partial s}{\partial \beta_i}\right|_{\beta=0} \quad = \quad \lim_{t\to\infty} \frac{1}{t}\left\langle \Phi_i^t \right\rangle \;=\; \left\langle \phi_i \right\rangle\,, \tag{29}$$

The flight time and the logarithm of the orbit instability are additive along a trajectory as requested so a brute idea could be to obtain the characteristic average lyapynov exponent through division of the characteristic logarithm of instability with the characteristic time.

In practice we end up doing evaluations of the truncated zeta function and use these to estimate the value of the zeta function derivatives with respect to β and s. using the expressions

$$1/\zeta = G = \prod(1 - t_p) \tag{30}$$

and

$$t_p = \frac{e^{\beta \ln|\Lambda_p| - sT_p}}{|\Lambda_p|} \tag{31}$$

The only difficult thing left is the matter of proper truncation of the zeta function expression (making sure to involve the right amount of shaddowing orbits. (sorry about the relaxed style above – time is running negative.)

5 Symbol Dynamics

As discussed above a full set of prime cycles up to a certain order can be used to determine most of the dynamical characteristics of a chaotic system, but such a set of prime cycles is not necessarily easy to find: We need a systematic way of describing the orbits to eliminate doublets and identify missing prime cycles. Furthermore we need some concept of cycle order that corresponds reasonable with cycle importance. These aims are normally pursued through the construction of a suitable set of symbol dynamics for the system – a finite or countable alphabet is conceived, and subsequently a sequence of these symbols is attached to every orbit. The matter of constructing this alphabet deserves some discussion.

Before starting a presentation of the different kinds of symbol alphabets, we should recall that our Stadium billiards have a C_{2v} symmetry. Symbol dynamics based on the full system have the advantage of being easy to deal with conceptually but topologically similar orbits will have different symbol sequences attached to them[4], and their multiple appearance in the zeta functions will neccesitate cumbersome symmetry factors. The fundamental domain implies other problems – they are conceptually more involved, and one have to look out for different orbits special symmetry properties (boundary cycles[5] etc). For the uses of periodic orbit theory – the characteristic time and instability – involved symmetry considerations proves to be irrelevant and will not be discussed further.

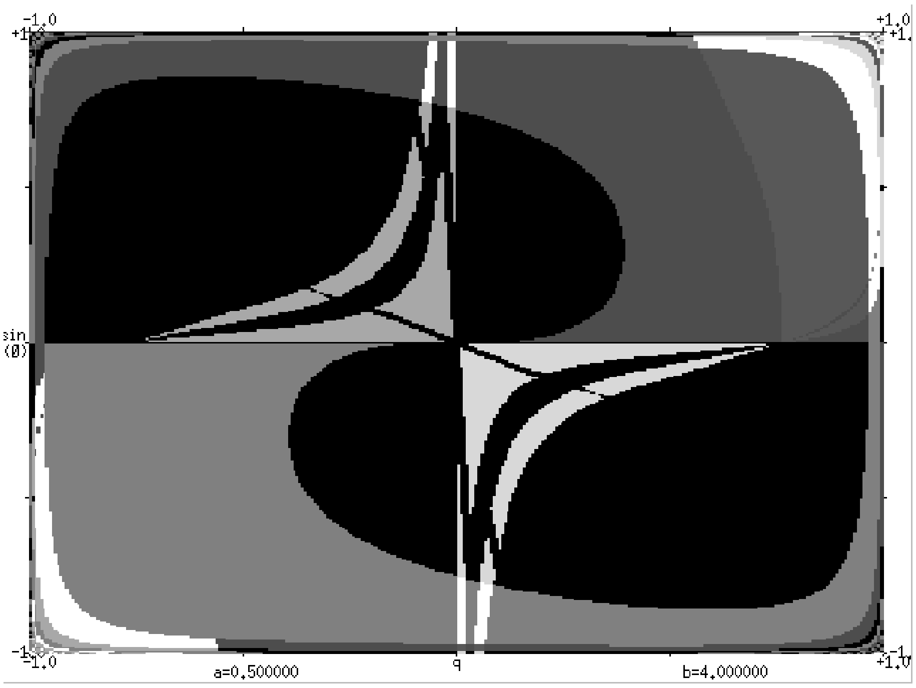

Figure 5: Symbol plane for a=0.5 , b=4

5.1 Choosing a Symbol Alphabet

Since the Soft wall stadium is not a standard system, no symbol alphabet proposals are to be found in the literature for this particular system. Instead we'll seek inspiration in the alphabets proposed for the Hard wall stadium and see if they satisfy reasonable expectations. The following properties should be considered:

Existence Do symbol sequences exist for all possible cycles.

Uniqueness No two topologically distinct cycles should have the same symbol sequence.

Geometric pruning rules Independent of system parameters certain symbol sequences are unphysical (no such cycle exist) for some types of symbol dynamics.

Dynamical pruning rules Independent of symbol alphabet some cycles existence depends on the system parameters - causing pruning fronts in the symbol

[4] and they will have to be determined separately - an important consideration in a system such as ours where every prime cycle has to be found by hand using 10-30 minutes

[5] ignoring the marginally stable vertical cycles we have only one boundary orbit - the horizontal one at the x-axis

dynamics. It is preferable if cycles whose existence have similar dependence on system parameters have symbol sequences close to one another.

Experimental Applicability As opposed to the Hard wall system[**?**, Han95a] we have no easy way to obtain cycles given a symbol sequence. We can just simulate trajectories and seek the ones that bite their own tail. We're left with a chain of points on this orbit in full domain and from this information the proper symbol sequence should be obtainable without too big sensitivity to the minor imprecision we are bound to have.

The literature proposes the following symbol alphabets for the Hard wall Bunimovich stadium

BQ Full stadium symbol alphabet proposed by Biham and Quale [**?**] based on a classification of wall-bounces after which section is hit and which way is turned.

AK Full stadium symbol alphabet proposed by Akiyama and Koga [Aki94] based on classification of inter-bounce trajectories - rather involved.

CHUH Biinfinite Unfolded Half stadium symbol alphabet proposed by Cvitanovic and Hansen[Cv95a] counting bounce-number separately in the semi circle and the straight wall sections. Parity based on rotation orientation and inter cell flying direction

CHUQ Biinfinite Unfolded Quarter stadium symbol alphabet proposed by Cvitanovic and Hansen[Cv95a] counting bounce numbers as above, parities based on number of bounces on the x-axis.

CHQ Biinfinite Quarter stadium symbol dynamics proposed by Cvitanovic and Hansen [Cv95a] related to CHUQ but every bounce gets its own symbol. The Geometric pruning rules are somewhat involved.

'modCHUQ' 'Half infinite' modified CHUQ that I've ended up using in this project after much experimentation. Described in detail below. (this is of course NOT from the literature)

All of the above methods are based on locating and counting bounces - that is points where the trajectory meets the Stadium boundary. In the Soft wall stadium such encounters are only found in the marginally stable vertical orbits and in trajectories that at some point follows a radius in and out of the semi circle. In all other cases we have soft bounces (see fig 1). If we want to implement the symbol alphabets above in a way that gives a similar labelling of similar orbits in respectively the hard wall and the soft wall case – this concept of a bounce. Therefore any local maximum of r along the trajectory is considered a bounce[6]

5.2 The modCHUQ symbol alphabet

With the concept of bounce settled we can now – at every crossing of the line separating the quarter circle and the rectangular section[7] – count the bounces during

[6]Of course one could demand that the bounce should have a certain minimal r-value or a certain minimal radii of curvature - but what minimum would be the proper one? I have experimented in this direction but with no obviously succesfull results.

[7]the main line of Poincare cuts - remember we're in the fundamental domain

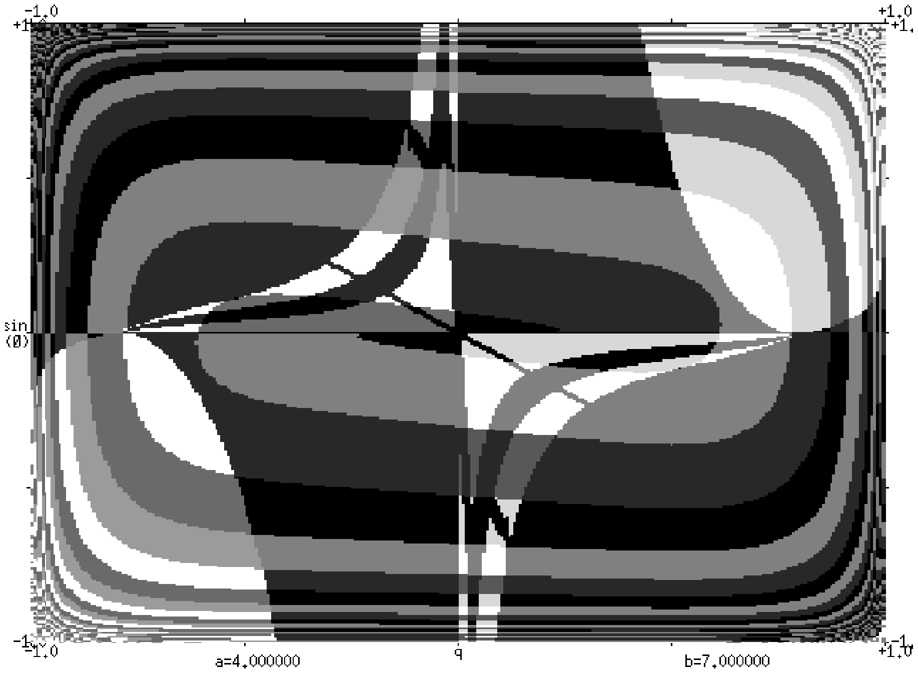

Figure 6: Symbol plane a=4.0 b=7.0 - identical with front page

this passing of the respective regions. When entering the semi circle we get a symbol-pair (C, R) :

$$
\begin{aligned}
c &= \sharp\text{bounces in semi circle dur. last pass} \\
r &= \sharp\text{bounces in rectangular region dur. last pass} \\
s_c &= \sharp x - \text{axis crosses since semi circle exit} \\
s_r &= \sharp x - \text{axis crs betw. semcirexit and first rectan.wallbounce} \\
C &= (-1)^{s_c+1}(c-1) \\
R &= (-1)^{s_r} r
\end{aligned}
$$

The order of the orbit will be the number of such (C, R) pairs

I didn't settle on this symbol alphabet until a week before the project termination so some of the graphs of earlier simulations may have slightly different sign expressions, but this should not seriously disturb the feel for the symbol plane.

Comparison of the symbol plane of the soft wall stadium with that of the hard wall case reveals some interesting differences:

(See the hard wall stadium symbol plane on figure 3 and 4 in the exam project of Jonas Lundbæk Hansen - note -my sinfi sign convention are opposite of his)

The whispering gallery (orbits with many bounces in the semi circle) is absent in the soft wall stadium dynamics. No more that 2 bounces[8] seems to be allowed for the values of b ($b <= 8$) studied systematically in this project. the 2-bounce blob in each corner is extended with the strange vertical double structure for low values of q (in the middle); this is unparallelled in hard wall case and seems to indicate the existence of a half-bounce on the way to the real bounce nearer the semi circle rim. This structure changes if different or more restrictive bouncing rules but it doesn't disappear. This seems to indicate significant differences in the dynamical pruning

[8]thus the symbol dynamics are no longer Biinfinite

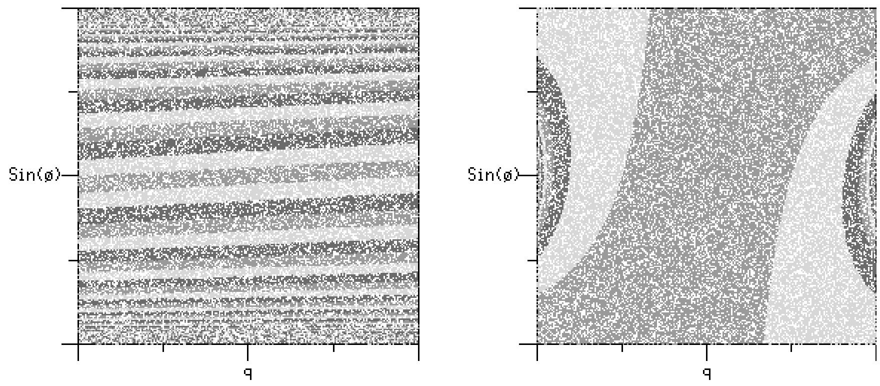

Figure 7: The Poincare section for a flight in the a=10 hard wall stadium. from Jonas Hansens project (please note that my sinfi sign convention is opposite of his)

rules. The differences in the *straight wall bounce* symbol plane are not so pronounced but for higher values of $|q|$ there is a significant deformation of the stripes. This is because a trajectory up near the edge of the potential cannot help being bended off by the potential no matter its momentum direction. the momentum is numerically small and will not be able to compete with the bending effect of the potential, wherefore the central part of the stadium cannot be crossed without bounces. (note the central stripe represents orbits with on mid piece bounces where as the outer stripes represent many mid piece bounces).

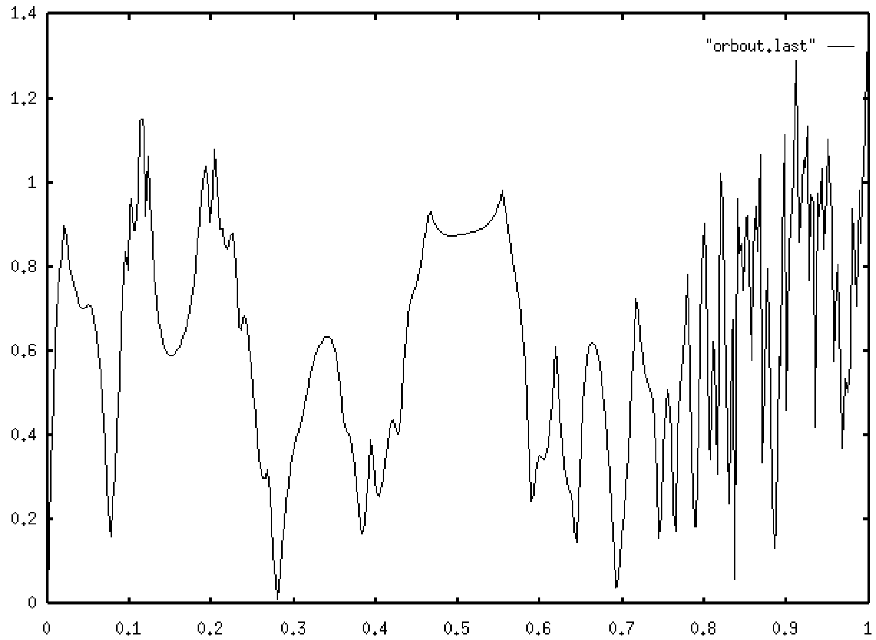

Figure 8: Phasespace end to end distances after 3 iterates. a=1 b=6 sin(ø)=0 , q varying in poincare cut type 3.

In its present implementation the algorithm has a problem with orbits crossing through $(a, 0)$ – the semi circle centre (did the trajectory cross the x-axis in or out of the semi circle. This can be fixed but I hadn't got the time. Furthermore I've found out that certain symbol sequences are not always unique in the present implementation – a order 3 prime cycle can have the same symbol sequence as a tipple repetition of a order 1 prime cycle. Finally I've seen indications of a pair of twin-orbits : same symbol-string, same order, similar but consistently slightly different parameters. This may be real or it might be one fake minimum and a true orbit. The symbol sequences of different periodic orbits can be seen in the last column in appendix C.

5.3 How to find the prime cycles

Now we know how to extract the relevant information from a given periodic orbit (order, pass-time, length, instability, parity and symbol sequence) we just need to find them. All prime-cycles have to visit the semi circle. We start trajectories at some value of $(q, \sin(\phi))$ – a point in the type 1 poincaré cut and minimises the distance to the first, second, third or fourth return of the trajectory to this poincaré cut (depending on what order prime cycle we're looking for). *This method has severe limitations.* Using 2 dim simplex algorithm search from Numerical Recipes[Pre92]. Kai Hansen proposes search along the local tangent directions of the stable and unstable manifolds[Han95].

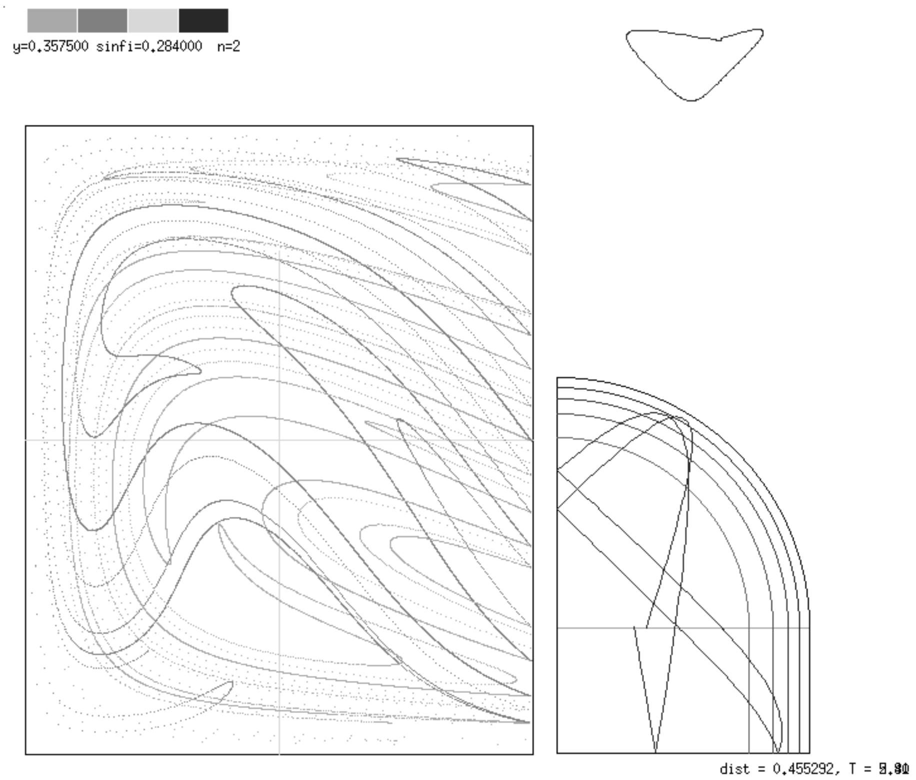

Figure 9: x-interface of periodic orbit search program, inclucing the fundamental domain picture of crossing stable and unstable manyfolds

I've used the stable and unstable manifolds as visual aids in my prime cycle search, but I've not had time to implement this properly superior search strategy (I'll get to the manifolds in next section). The minimisation landscape seems to be dominated by highlands with some relatively broad valleys (less unstable cycles have broad basins of attraction, whereas the more unstable cycles have extremely narrow basins of attraction) this search method is bad for order> 1. Many of the lower order orbits can be expected to have some nice symmetry properties.

cycles that are Symmetric or antisymmetric around the y-axis are numerous. Time symmetry yields the possibility of cycles starting at the rim of the semi circle - these are bound to cross the semi circle centre with some angle. These three symmetries makes separate types 1 parameter search possible and most of the identified periodic orbits have been found this way. the one parameter searches are succesfull up to order 3-4 but not beyond. A better method would be to minimise n first order iterates with mutually approaching endpoints. This method would work for higher n, but demands involved programming ($2n$ parameter search). This method has been beyond the scope of this project. (For more information on programs etc – consult appendix B).

6 Manifolds

The Unstable Manifolds[Ott92] of the horizontal orbit $(0,0)$ has been subject of some study during. It is obtained by starting a trajectory at a distance of 1.0×10^{-8} from $(0.0, 0.0)$ in the type 1 Poincare cut letting it iterate 5-6 times to track it in on the 1-dimensional manifold. Making a linear interpolation between the two next iterations (We're still so close to the periodic point that the manifold can still be assumed to be linear – directed along the poincaré cut image of the unstable eigenvector). Some number of points along this line are now recorded, and all of them are iterated a suitable number of times (5-12) to reach significant parts of the poincaré cut. The trajectory passes through the other poincaré cuts (type 2 and 3), are also recorded.

The stable manifold is obtained through time reversal of the orbits on the unstable manifold. Note that poinc.cut type 1 maps to type 2 in a time reversal and vice versa. thus

$$(q_1, \sin(\phi)_1)_{stable} = (q_2, -\sin(\sin(\phi)_2)_{unstable} \tag{32}$$

Periodic points (of other cycles) can be expected to lie at the intersections of stable and unstable manifolds[Ott92], and I have used them to guide my 2d search. If these combined manifold pictures are given for some set of neighbouring system parameter values, the appearance and disappearance of manifold crosses can reveal dynamical pruning rules. The round turns in the soft stadium manifolds correspond to the kinks in the hard wall stadium manifolds. Tracing the points of maximal curvature as functions of system parameter values would be a interesting way to quantify the dynamical pruning rules. This has been beyond the scope of this project.

7 Result of periodic orbit theory

The application of dynamical zeta function/Fredholm determinant methods might seem somewhat silly considering our insufficient insight in the set of periodic orbits. It is not unlikely that the first missing orbit has only 4 or 5 bounces, which should mean that all the higher order orbits available are worthless. (they have been found mostly for the purpose of demonstrating the reach of our search methods, which has taken up much of the project time). Furthermore many of the orbits available crosses the semi circle centre, where the present implementation of the symbol dynamics algorithm has problems - meaning that some of the total bounce numbers may be off by 1 or 2[9]. This can seriously mess up the orbit shadowing systematics and thus whatever result we get from application of the theory presented in section 4 should not be expected to have a narrow error margin. To get the two slopes of

[9] for example the horizontal orbit which would be expected to have the symbol dynamics $(0,0)$ which corresponds to a bounce number of 1, is given the value 2

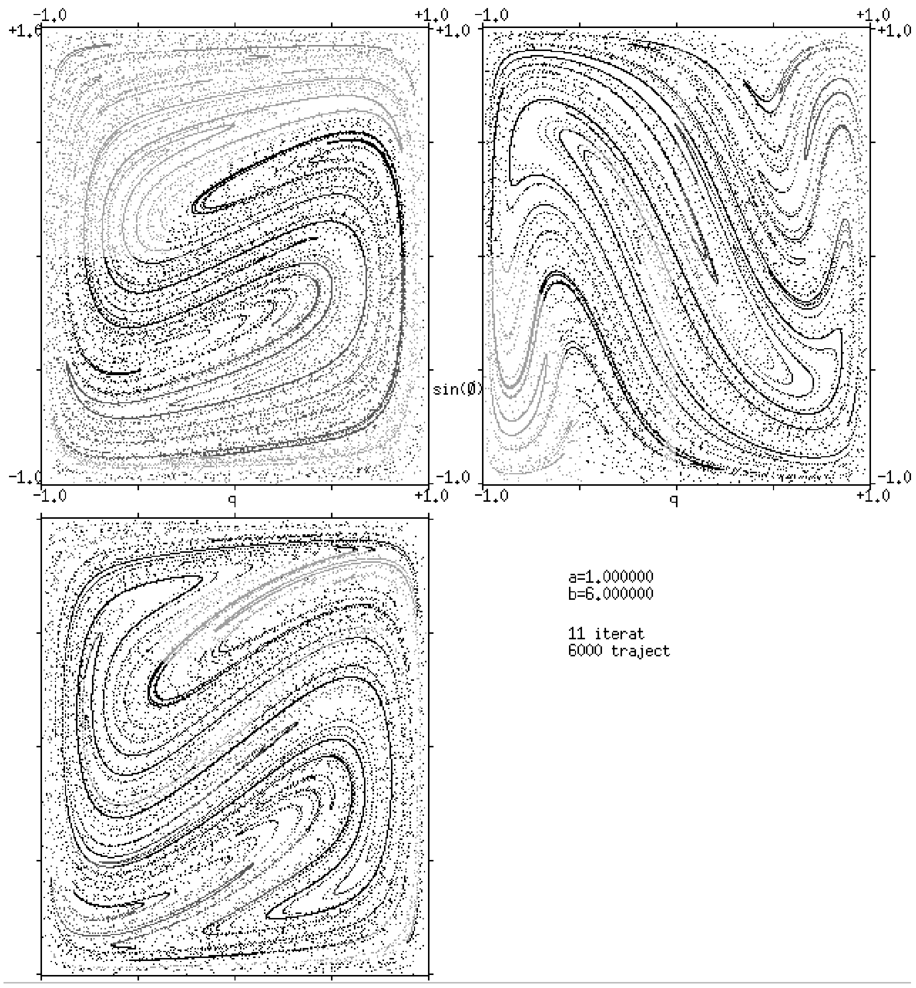

Figure 10: Manifolds corresponding to poincare cuts type 2,1 and 3 , a=1 , b=6

the zeta function derivatives $\frac{\partial(1/\zeta)}{\partial\beta}$ and $\frac{\partial(1/\zeta)}{\partial s}$ at $(\beta, s) = (0, 0)$ I've used a modified version of Jonas L Hansens corresponding program.

The values obtained for the average lyapunov exponent of the system at parameters $(a = 1.0, b = 6.0)$ has been calculated using all available prime cycles up to 4,5 and 6 bounces (which is equivalent to 'assuming' that only orbits of bounce numbers 5,6 respectively 7 and above are missing. Both the instability factor types have been attempted used (calculated respectively with linear 2×2 matrix and the diverging orbits methods). The results were at follows

$$\begin{array}{lll} n \leq 4 & \lambda_m = 0.398 & \lambda_d = 0.384 \\ n \leq 5 & \lambda_m = 0.398 & \lambda_d = 0.383 \\ n \leq 6 & \lambda_m = 0.397 & \lambda_d = 0.382 \end{array} \tag{33}$$

Trying the obviously absurd assumption, that we have all orbits $n \leq 11$ we get $\lambda_m = 0.359$. The error of the bounce number assigned to orbit $(0,0)$ has already been discussed. I also tried to insert the 'correct' value 1 which gave the values $n \leq 4 \quad \lambda_m = 0.401 \quad \lambda_d = 0.399$ that the diverging orbit method generally gives lower values should not be surprising; even though the inter orbit vector $\partial\vec{x}$ gets some time to direct itself in the direction of the unstable eigenvector of the Jacobian (one Poincare cut iteration) it can not be expected to be fully tracked in - yielding too low instability factors of the prime cycles. the too low $n \leq 11$ of λ_m indicates, that many orbits of bounce number 11 are missing – *surprise, surprise.*

Comparison with the value $\lambda = 0.454$ of Jonas L Hansen yields that the soft wall values are lower as should be expected - but keep in mind that where as Jonas's particle moves with constant speed 1, the soft wall stadium particle moves with a varying speed between 0 and $\sqrt{2}$, which diminishes the comparability of the characteristic times.

Comparing with the results displayed in section 3 based on random initial conditions, gives that the 'stupid method' value is somewhat lower value $\lambda = 0.32$. Generally this value should be expected to be lower because of the random initial condition methods sensitivity to the vertically bouncing orbits and because we have the usual problem, that the dual orbit method needs time to track the instability direction. Still the 20improvement – but we already knew this.

8 Conclusion

It has been quite a challenge to deal with a system that has proven hard to simulate (especially when calculations include the discontinuous second derivative), a system with unknown/undefined symbol dynamics that had to be explored in a spirit of scepticism and a system that is rather unwilling to reveal its periodic orbits. Calling this kind of system hard is tempting after 6 weeks of late nights and endless programming (causing a total of 25 widely differing programs). A more correct attitude might be a 'welcome to the real world', because these problems are the ones one should expect to encounter when trying to apply periodic orbit theory. This is not to say that it wouldn't be worth the troubles - if 1 or 2 more weeks had been available sets of cycles could have been determined for several values of a and b, now that the programs are finished and working, and for similar reasons further insight in the symbol dynamics and pruning fronts should not be too hard to obtain. Periodic orbit theory is a interesting tool, but with systems that approaches anything real, one should be prepared to put in a lot of time and effort before getting any quantitative results.

References

[Ott92] Edward Ott, *Chaos in Dynamical Systems*, (Cambridge University Press 1993).

[Pre92] W.H. Press, B.P.Flannery, S.A.Teukolsky and W.T.Vetterling, *Numerical Recipes in C, Second Edition*, (Cambridge University Press 1992).

[Cvi95] P. Cvitanovich et al, *Classical and Quantum Chaos, a Cyclists Treatise.*

[Han95] K.T. Hansen, *Alternative method to find orbits in chaotic systems*

[Cv95a] P. Cvitanovich and K.T. Hansen, *Symbolic Dynamics and Pruning Fronts for the Stadium Billiard*

[Bih92] O.Biham, M.Kvale *Unstable Periodic Orbits in the Stadium Billiard*, (Phys. Rev. A,46,10,p.6334, (1992)).

[Aki94] S.Akiyama, S.Koga *Statistical Properties of Unstable Periodic Orbits in the Stadium Billiard*

[Tan92] G.Tanner, *Phd Thesis*, (Freiburg 1992)

[Eck92] B.Eckhardt, D.Wintgen *Indices in classical mechanics*, (J.Phys. A:Math. Gen. 24 (1991) 4335-4348).

[Han95a] J.L.Hansen *Lyapunov Exponents for the Stadium Billiard* (Exam Report - Classical and Quantum Chaos - Aug 1995)

9 Appendices

9.1 Appendix A : Simulation Methods and their Complications

Lack of time forces me to make this short. Both Burlish Stoer (originally recomnended by Kai Hansen) and fourth order Runge Kutta integration has been tested in the early phases of the experiment. (through modifications of the inplementations in Numerical Recipes) The BS method prooved to be very sensible to the discontinuity of the second deriv at the semicircle interface.

9.2 Appendix B : Programs

No time is left me for any kind of detailed description of the 25 different programs develoved over the project period, but I will be happy to demonstrate them to anybody interested.

Two programs from the early phases of the project implemented the two integration methods, contains x interface and monitoring of energy conservation

Test programs for the basic kinds of lyap exp calculation

programs to make statistics based

(there is no more time)

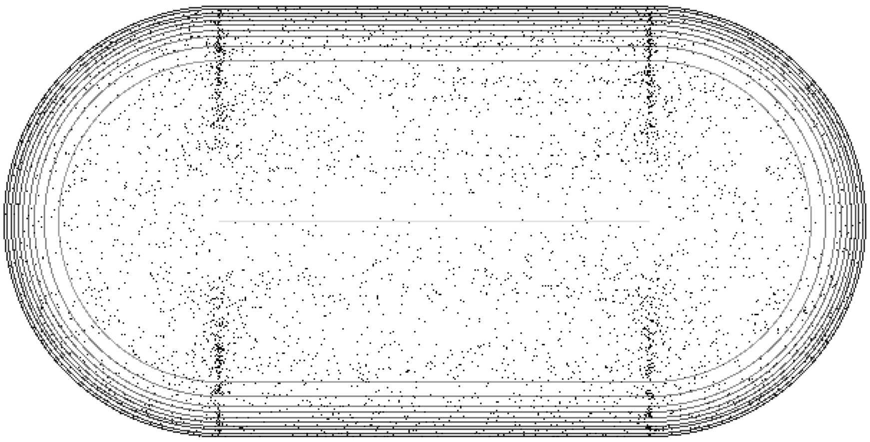

Figure 11: points of interstep stops of the Burlish Stoer integration method – note concentration at discontinuity line.

9.3 Appendix C : Periodic orbits

These are the 50 periodic orbits found for $a = 1.0$, $b = 6.0$:

nr	q	sin(Ø)	bn	sgn	time	length	instab-1	instab-2	symb.dyn.
1	0.000000	-0.000000	2	+	3.131529	3.999811	4.810836	4.856503	(-1,0)
1	0.484425	-0.314602	3	-	3.301017	4.260622	2.605768	2.882969	(1,1)
1	0.000001	-0.739341	2	-	3.817637	4.741584	5.074589	3.485489	(0,1)
1	0.689749	0.865406	3	-	5.401073	6.582712	13.399864	9.500779	(-1,-1)
1	0.000005	-0.963481	4	-	6.998593	8.328650	14.274104	12.737490	(0,3)
1	0.668618	0.971217	5	-	8.695990	10.302236	25.773649	22.971539	(-1,-3)
1	0.768445	0.486466	2	-	4.027158	5.111266	0.580135	4.416807	(1,0)
1	0.000000	0.920922	3	+	5.345853	6.447879	10.175587	9.187440	(0,2)
1	0.673407	0.945518	4	+	7.021410	8.394849	19.696675	16.083858	(1,-2)
1	0.000000	0.979177	5	+	8.683626	10.262585	17.833231	16.468920	(0,4)
1	0.580213	0.991661	10	+	17.361866	20.337954	52.739433	75.028058	(1,-8)
1	0.000000	0.920922	3	+	5.345852	6.447878	10.175587	9.120999	(0,2)
1	0.000000	0.986589	6	-	10.381531	12.219964	21.250869	19.993974	(0,5)
1	0.000000	0.990655	7	+	12.085909	14.190008	24.713994	23.666588	(0,6)
1	0.000000	0.993120	8	-	13.793981	16.167686	28.216893	27.301052	(0,7)
1	0.000000	0.994725	9	+	15.504368	18.150353	31.745033	30.926884	(0,8)
1	0.000000	0.995828	10	-	17.216289	20.136457	35.301701	34.554327	(0,9)
1	0.000000	0.996619	11	+	18.929300	22.125062	38.925789	38.187319	(0,10)
2	0.353000	-0.017959	4	-	6.575225	8.445883	10.783360	12.525878	(0,1) (0,1)
2	0.302714	-0.577924	3	-	6.701038	8.537229	24.109428	21.871379	(0,0) (0,1)
2	0.211155	0.801201	5	-	9.136087	11.176797	49.096666	52.329381	(0,2) (0,-1)
2	0.329533	0.826444	6	+	10.763977	13.039548	66.285714	67.791746	(0,3) (0,-1)
2	0.416645	0.841560	7	-	12.432170	14.961289	10.882641	21.240078	(0,4) (0,-1)
2	0.043211	0.964316	9	+	16.158927	19.265822	167.994616	486.900486	(0,3) (-1,-3)
2	0.446435	0.400617	4	-	7.999372	10.041477	0.389947	17.122922	(0,2) (0,0)
2	0.390867	0.940387	10	+	17.414307	20.630984	85.778625	85.221275	(0,6) (0,-2)
2	0.474683	0.943200	10	-	17.348504	20.546510	162.225546	128.449651	(1,-5) (0,-2)
2	0.560615	0.945217	9	-	15.719023	18.698926	461.745960	329.796072	(-1,-3) (1,-2)
2	0.942004	0.859338	7	-	12.432585	14.986270	156.076189	62.589505	(-1,-1) (1,-2)
2	0.000000	0.466744	4	-	6.872906	8.789901	11.958991	12.768306	(0,1) (0,1)
2	0.000000	0.831727	5	+	9.190382	11.299211	70.975663	54.033163	(0,1) (1,-1)
2	0.000000	0.938521	7	+	12.362222	14.839035	209.127706	148.370435	(0,2) (-1,-2)
2	0.000000	0.981757	11	+	19.072090	22.508662	572.872558	491.918868	(0,4) (-1,-4)
2	0.389342	-0.934327	6	-	10.771377	13.073180	116.025547	78.209478	(0,-1) (-1,-2)
3	0.277688	-0.005111	8	+	9.845610	12.665115	24.912570	46.475235	(-1,1) (1,1) (0,1)
3	0.364923	-0.520956	4	-	9.753420	12.490111	90.855257	46.265147	(0,0) (0,0) (0,1)
3	0.000000	0.145070	4	-	9.782322	12.500151	113.722732	94.812870	(0,0) (0,1) (0,0)
3	0.180653	-0.658936	7	+	10.622778	13.494668	78.966012	40.038408	(0,-1) (-1,1) (0,1)
3	0.178837	0.175967	5	+	9.911494	12.709540	4.057424	54.042842	(0,1) (0,1) (0,0)
3	0.298294	0.284876	5	+	10.483605	13.255803	93.941214	117.609573	(0,1) (0,1) (0,0)

3	0.378152	0.350588	6 +	11.946742	15.007019	69.309134	172.668845	(0,1) (1,-1) (0,0)
3	0.000000	0.776701	7 +	12.948926	15.918498	235.395875	295.607603	(0,1) (0,2) (0,-1)
3	0.000000	0.793518	8 -	14.571783	17.779676	265.253514	343.361741	(0,1) (0,3) (0,-1)
3	0.000000	0.932774	13 -	22.758006	27.082789	32.031757	10.245999	(0,2) (0,6) (0,-2)
4	0.076362	-0.000008	8 -	12.895984	16.497042	479.781972	421.094160	(-1,0) (0,1) (0,0) (-1,1)
4	0.000000	0.107559	7 +	13.018510	16.692415	85.072929	217.524189	(0,0) (0,1) (1,1) (0,0)
4	0.000000	0.175362	6 +	13.545024	17.206686	381.328127	462.537313	(0,0) (0,1) (0,1) (0,0)
4	0.000000	0.228146	7 +	14.973801	18.940306	25.255828	371.798204	(0,0) (0,1) (1,-1) (0,0)
4	0.000000	0.540933	9 +	13.536136	17.357646	19.078456	84.168441	(0,1) (0,1) (1,1) (0,1)
4	0.000000	0.619094	7 +	13.500692	17.192511	213.660912	351.440434	(0,1) (0,0) (1,0) (0,1)

in the zeta function calculations the values of the first instabilities that are below 1 (clearly wrong) are replaced by the diverging orbit instabilities that can normally be considered to be of the right magnitude.

[EOB]